Laser-produced gaseous plasmonic resonators

Roberto A. Colón Quiñones, Thomas C. Underwood, and Mark A. Cappelli

Citation: Physics of Plasmas **25**, 113501 (2018); doi: 10.1063/1.5054022
View online: https://doi.org/10.1063/1.5054022
View Table of Contents: http://aip.scitation.org/toc/php/25/11
Published by the American Institute of Physics

Laser-produced gaseous plasmonic resonators

Roberto A. Colón Quiñones,[a] Thomas C. Underwood, and Mark A. Cappelli
Stanford Plasma Physics Laboratory, Stanford University, Stanford, California 94305, USA

(Received 28 August 2018; accepted 17 October 2018; published online 1 November 2018)

We study the electromagnetic scattering properties of a gaseous plasma resonator generated by laser-induced gas breakdown. A simple analytical model is used to describe the scattering resonance of these near-ellipsoidal plasmas and its dependence on their eccentricity and intrinsic plasma properties. This dependence is investigated through Ku band transmission experiments of a waveguide with an embedded single plasma element and optical diagnostics of the laser-induced plasma. The described resonator has the potential to be used as the building block in a new class of metamaterials with fully three-dimensional structural flexibility. *Published by AIP Publishing.*
https://doi.org/10.1063/1.5054022

I. INTRODUCTION

The electromagnetic (EM) properties of most natural materials are dictated by the resonances of their constituent atoms, which are typically ~1 Å in size. Because of the small spacing between these atoms, many EM wavelengths of engineering interest (vacuum ultraviolet waves or longer) only probe their average or effective properties. A metamaterial (MTM), i.e., an artificial material engineered to exhibit EM properties not readily found in nature, follows the same principle.[1] The resonantly active elements in MTMs and their spacing are designed to create an effectively homogeneous medium with engineered EM properties. Such a medium is achieved when the spacing between the constituent elements is smaller than a quarter of the guided wavelength.[2] The ability to create MTMs with exotic effective properties has led to the formation of the very active field of transformation optics where MTMs of spatially varying refractive indexes are used to steer EM waves in unusual ways to achieve phenomena such as negative refraction, perfect lensing, and optical cloaking.[3]

In recent years, a significant portion of research in this field has focused on exploring the tunability of these phenomena. Tunable MTM devices have exploited the electromechanical, electro-optical, liquid-crystal, phase-change, and superconducting response of their constituent elements.[4] A class of potentially tunable elements that have been largely overlooked are gaseous plasmas, which can be incorporated into more traditional MTMs to form composite periodic structures with tunable features.[5] The tunability of these structures stems from the dispersive nature of plasmas arising from their variable electron density (n_e) and electron momentum transfer collision frequency (γ). These two plasma properties are in turn controlled by the energy invested by the ionizing source and the pressure/composition of the gas.

The majority of previous research related to plasma MTMs has focused mainly on the development of composites that integrate plasmas into metallic resonant structures[6–14] or into dielectric resonator arrays.[15,16] Waveguiding MTM structures composed exclusively of laser-induced plasma (LIP) filaments have also been proposed[17] but have yet to be realized experimentally. This article reports on a gaseous plasma resonator that could potentially be used as the building block for an all-plasma MTM. Specifically, this study describes the EM properties of a LIP resonator which is generated by tightly focusing the fundamental output from a pulsed, high-energy laser through a lens and into a gas[18,19] [see Fig. 1]. The sub-wavelength spheroid[20,21] with near-uniform n_e achieved after electron concentrations at the edge of the plasma have decayed[19] interacts with incoming radiation through excitation of low-order, electric-dipole resonances similar to those seen in metallic spheres.[22] These electric-dipoles are induced by the restoring force of the plasma boundary on the oscillating electrons.

For frequencies below the plasma frequency (ω_p), the collective scattering response of a MTM composed entirely of these plasmonic resonators results in a finite region of negative effective dielectric constant near the frequency of the excited surface mode (ω_0).[23] As shown in Fig. 2, this leads to a region of finite reflection, in contrast to the semi-infinite region observed in bulk plasmas. Potential applications of MTMs constructed from arrays of these LIPs include, but are not limited to, highly tunable reflective surfaces and negative-index mediums with fully three-dimensional structural flexibility. These MTMs are particularly suited for high-power microwave applications where traditional microwave components are shorted and remote generation is advantageous. Moreover, the plasma densities ($n_e \leq 10^{25}$ m^{-3})[19] and dimensions (size $\geq 10\,\mu$m)[21] achieved in these resonators

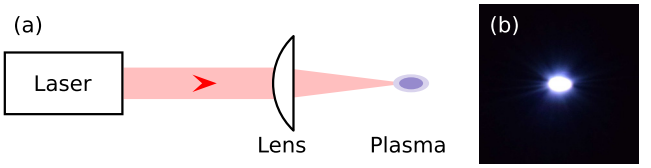

FIG. 1. (a) Experimental setup for generating a LIP. (b) Optical image of LIP generated in air at p = 1 atm.

[a]Electronic mail: racolon@stanford.edu

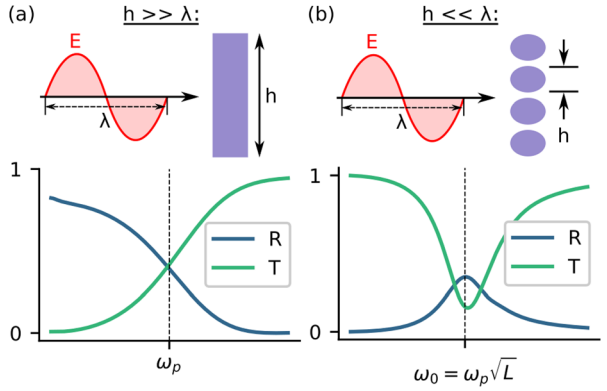

FIG. 2. (a) Reflectance (R) and transmittance (T) observed in bulk plasmas. (b) R and T observed in sub-wavelength plasmas.

translate to resonance frequencies as high as a few THz, making these MTMs potentially suitable for applications in the elusive THz gap.

II. THEORY

In this section, we derive a simple model describing the relationship between the resonance frequency and intrinsic plasma properties of these near-ellipsoidal resonators. An exact solution for the scattering fields from an ellipsoid, similar to the solution derived by Mie for the scattering fields from a sphere,[24] does not exist. However, for sub-wavelength particles, an electrostatic approximation can be used to obtain an approximate solution. Through such an approach, the polarizability of a sub-wavelength ellipsoid in a field parallel to one of its principal axes was found to be[22]

$$\alpha = v\frac{\epsilon - 1}{1 + L(\epsilon - 1)}. \tag{1}$$

Here, v is the volume of the ellipsoid, L is a geometrical factor dependent on the eccentricity and orientation of the ellipsoid, and ϵ is the dielectric constant of the plasma ellipsoid, which can be approximated by a Drude model,[22] i.e.,

$$\epsilon = 1 - \frac{\omega_p^2}{\omega^2 + i\gamma\omega}; \quad \omega_p = \sqrt{\frac{n_e q^2}{m_e \epsilon_0}}, \tag{2}$$

where ω is the incident radiation frequency, q is the electron charge, m_e is the electron mass, and ϵ_0 is the free space permittivity. For times after electron concentrations at the edge of the plasma have decayed, as required for resonance, the plasma is weakly ionized and γ can be approximated as[25]

$$\gamma = \beta \times 10^9 p\left(\frac{293}{T}\right). \tag{3}$$

Here, p is the gas pressure in Torr, T is the gas temperature in Kelvin, and β is a constant determined by the gas. This value of γ must be limited to be a small fraction of ω_0 to ensure that electrons in the LIP can oscillate freely and respond strongly to incident electric fields without being hindered by collisions with neutrals.

The absorption and scattering cross sections of these ellipsoids can be expressed in terms of the polarizability as

$$C_{\text{abs}} = k\text{Im}\{\alpha\}; \quad C_{\text{sca}} = \frac{k^4}{6\pi}|\alpha|^2, \tag{4}$$

where k is the wave number of the incident field.[22] These cross sections quantify the amount of electromagnetic radiation that is absorbed/scattered by the ellipsoids as a function of frequency. From Eq. (4), it is possible to see that there will be a resonance (i.e., a surface mode will be excited) in both cross sections at the frequency that makes the denominator of α vanish, i.e., when

$$\omega_0 = -\frac{i}{2}\left(\gamma + \sqrt{\gamma^2 - 4L\omega_p^2}\right) \tag{5}$$

or when $\omega_0 = \omega_p\sqrt{L}$ for a collision-less ($\gamma = 0$) plasma. Equation (5) highlights the tunable nature of the described gaseous plasma resonators. The dependence of ω_0 on ω_p and γ confirms its dependence on the energy invested by the ionizing source and the pressure/composition of the gas. The geometrical factor, L, is independent of the plasma properties, but for the prolate-spheroid shaped plasma generated by a laser focused to a circular beam waist, it could take on two different values depending on whether the electric field is incident parallel or perpendicular to the major axis of the spheroid. The geometrical factors for the two different cases are defined as

$$L_{\parallel} = \frac{1 - e^2}{e^2}\left(-1 + \frac{1}{2e}\ln\frac{1+e}{1-e}\right), \tag{6}$$

$$L_{\perp} = \frac{1}{4e^3}\left(2e + (e^2 - 1)\ln\frac{1+e}{1-e}\right), \tag{7}$$

where e is the eccentricity of the prolate spheroid.[22] By substituting Eqs. (2) and (6) [or Eq. (7)] into Eq. (5), the resonance frequency for a plasma spheroid with a major axis oriented parallel [or perpendicular] to the incident field was found to be dependent on n_e, γ, and e. It is important to recognize that for any finite collisionality case, Eq. (5) will have a complex solution. However, provided $\text{Im}(\omega_0) \ll \text{Re}(\omega_0)$, $\text{Re}(\omega_0)$ provides a good approximation for the resonance frequency of the resonator.

The conditions necessary for resonance in the Ku band (12–18 GHz) of the microwave spectrum were explored for a LIP with a major axis oriented parallel to the incident electric field. Only LIPs with dimensions $\leq$4 mm, which are commonly reported in the literature, were considered in order to satisfy the long wavelength criteria required by both Eq. (5) and the effective-medium limit. Figure 3 shows contour plots of the range of values of n_e and e which would lead to resonances inside this frequency range for a collision-less plasma. As shown in the figure, resonances could be achieved in the Ku band for resonators with densities ranging from $n_e \approx 5 \times 10^{18}$ m^{-3} to $n_e \approx 3 \times 10^{19}$ m^{-3}, assuming an eccentricity range of $0.1 < e < 0.9$. It is important to recognize that for the more realistic case of a collisional plasma, an increase in γ will lead to a redshift in these values of $\text{Re}(\omega_0)$, provided $\text{Im}(\omega_0) \ll \text{Re}(\omega_0)$.

III. OPTICAL EMISSION MEASUREMENTS

Optical emission measurements were carried out to determine if values in this range of n_e and e could be

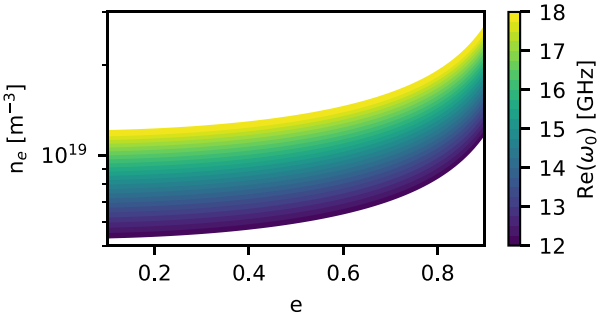

FIG. 3. Range of values of n_e and e, leading to resonance in the Ku band for the case where the incident electric field is parallel to the major axis of the resonator and $\gamma = 0$.

achieved for a LIP. A schematic of the experimental setup used for Stark-broadened emission and plasma eccentricity measurements is provided in Fig. 4. As shown in the figure, the collimated output pulse generated by a Q-switched Nd:YAG laser (wavelength: 1064 nm, energy: ∼180 mJ/p, repetition rate: 10 Hz, pulse duration: ∼10 ns, and beam diameter: ∼10 mm) was focused through a plano-convex lens (diameter: 30 mm and focal length: 40 mm) to produce a plasma spheroid. The plasma was generated in a 93%N_2/7%H_2 gas mixture at a relatively low pressure of 20 Torr to minimize electron-neutral collision losses. It is worth noting that the intense heating of the laser at the focal spot leads to hydrodynamic expansion of the gas in the form of a blast wave.[18,19] This means that the value of the gas P/T ratio, i.e., the gas density, behind the shock will be lower than the initial value. Hence, the value of γ obtained by substituting initial gas conditions in Eq. (3) will be an overestimate of the actual value.

The time evolution of n_e was determined by measuring the Stark broadening of the LIP's Hα emission line, and the eccentricity was determined from gated images of its broadband emission. The LIP was imaged at the entrance slit (width = 60 μm) of a Jobin-Yvon U1000 double monochromator where a dual holographic 1800 groove/mm grating

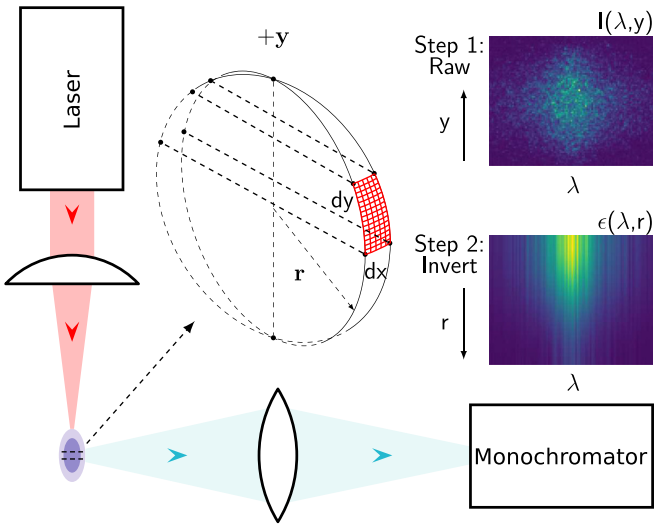

FIG. 4. Schematic of the experimental setup for Stark broadening measurements, together with sample images of the LIP's chord-integrated intensity and Abel-inverted emissivity.

dispersed the light, which was then imaged onto a Princeton Instruments PI-MAX intensified CCD camera. A wavelength calibration factor of 0.0568 Å/pixel and a height calibration factor of 0.0307 mm/pixel were determined by placing a mercury spectral lamp at the focus of both the plasma-generating lens and emission-collecting lens. Two closely spaced Hg lines (576.961/579.067 nm) provided the wavelength calibration, while two 1 mm black strips taped onto the mercury lamp 1 mm apart, provided the height calibration. The instrument broadening was determined using diffuse scattering from a HeNe laser, establishing a baseline for deconvolution from broadening due to the plasma. The camera was triggered simultaneously with the laser Q-switch and gated to a 150 ns exposure so as to capture the time evolution of the plasma emission.

An Abel transformation was used to determine the radial profiles of the Hα line spectral emission from the chordwise integrated emission intensity, i.e.,

$$\epsilon(r) = -\frac{1}{\pi}\int_r^R \frac{dI(y)}{dy}\frac{dy}{\sqrt{y^2 - r^2}}. \tag{8}$$

Here, $I(y)$ is the experimentally measured, chord-integrated spectral intensity, R is the radius at which the measured intensity reaches the background level, and $\epsilon(r)$ is the calculated radially varying spectral emission coefficient. Given that the size of the plasma was larger than the monochromator's entrance slit, only light from an infinitesimal slab at the center of the LIP was used in this inversion. A schematic showing the y and r coordinates in this infinitesimal slab can be found at the center of Fig. 4. To carry out the inversion of Eq. (8), we used the Nestor-Olsen method, i.e.,

$$\epsilon_k(r) = -\frac{2}{\Delta y \pi}\sum_{n-k}^{N-1} I(y_n) B_{k,n}, \tag{9}$$

where the integers k and n are the position indices of the radial and vertical intensities, Δy is the distance between adjacent experimental data points, and $B_{k,n}$ are the weighting coefficients.[26–28] The Abel transform is highly sensitive to the symmetry of the measured integral data. Accordingly, the measured intensity was symmetrized about the centroid of the Stark broadened Hα emission line. Each vertical slice of the symmetrized data (see top-left inset on Fig. 4) was then inverted (see bottom-left inset on Fig. 4). A Voigt profile was then fit to the reconstituted spectral emission profile $\epsilon(\lambda, r)$. The Lorentzian component of the Voigt fit is attributed to the Stark broadening, the width of which gives n_e using an empirical correlation for the H_α Stark broadening rate.[29]

A plot of the time evolution of the radially averaged n_e resulting from these measurements is shown in the top panel of Fig. 5. As expected for the pulsed laser conditions, n_e in this plasma peaks at early times and decays through a combination of recombination and diffusion.[19] The data are presented as a function of Δt, which was the delay time between the laser Q-switch trigger and the time the measurement was taken. Data are only presented for the first ∼2.5 μs due to a drop in Hα line intensity below the detection limits of the

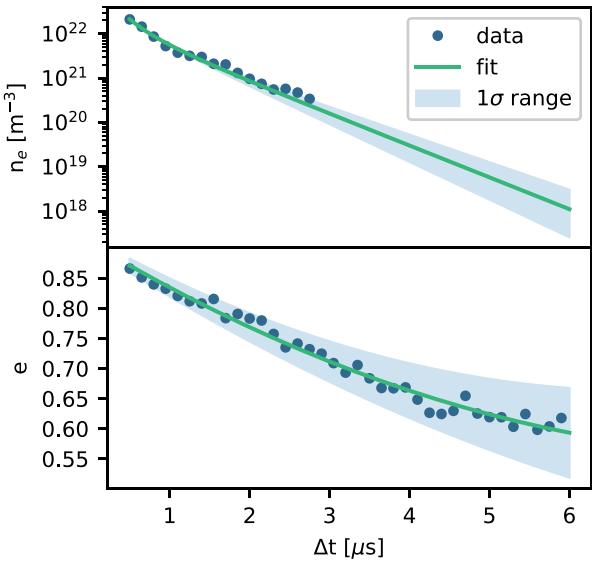

FIG. 5. Time evolution of n_e and e as measured by optical diagnostic experiments.

camera at later times. This drop is attributed to the relatively low gas pressure set to minimize electron-neutral collisional losses in subsequent microwave scattering experiments. To determine the time at which n_e would reach values that would lead to resonance in the Ku band, the data were extrapolated using a recombination/diffusion model, i.e.,

$$\frac{dn_e}{dt} = -\alpha n_e^2 - \frac{n_e}{\tau}. \tag{10}$$

Here, α is the recombination coefficient and τ is the characteristic diffusion time scale. Using a non-linear least squares regression, an optimal fit was found for $\alpha = 9.235 \times 10^{-17}$ m^3/s and $\tau = 0.606$ μs. The resulting fit is also shown on the top panel of Fig. 5 together with a one standard deviation (σ) interval envelope. As seen in the figure, an extrapolation of this fit to later times shows that the radially averaged n_e reaches values that would lead to resonance in the Ku band [see Fig. 3] for an approximate time range of 4.1–5.0 μs (1σ range: 3.6–5.6 μs).

The time evolution of the eccentricity was measured through gated images of emission from the LIP captured by bypassing the monochromator and focusing the broadband image of the plasma directly on the same (but repositioned) intensified CCD camera. The camera was triggered simultaneously with the laser Q-switch and gated to a 150 ns exposure so as to capture the time evolution of the plasma emission. Figure 6 shows a sequence of 5 mm × 5 mm images obtained through this method. Given that these images were primarily generated by light emitted through recombination radiation and excitation of neutral species throughout the plasma, the images provided a good estimate for the geometry and eccentricity of the resonators. The images in Fig. 6 show a plasma expanding almost symmetrically along the light cone and away from the focus, achieving a near-ellipsoidal shape after ~2 μs.

The resulting time evolution of e measured from a larger group of these 150 ns exposure images can be found in the bottom panel of Fig. 5. The figure shows that at times where n_e reaches values that would lead to resonance in the Ku band, the spheroid eccentricity is in the range of 0.62–0.66 (1σ range: 0.54–0.72). This further reduces the range of n_e values that could lead to resonance in the Ku band and in turn the approximate time range at which these resonances are expected to 4.4–4.9 μs (1σ range: 3.9–5.5 μs). The images in Fig. 6 show that at these times, the plasma spheroid has a major axis of length ~4 mm, which is below $\lambda/4$ for all Ku band wavelengths, satisfying the long wavelength limit required by both Eq. (5) and the effective-medium limit.

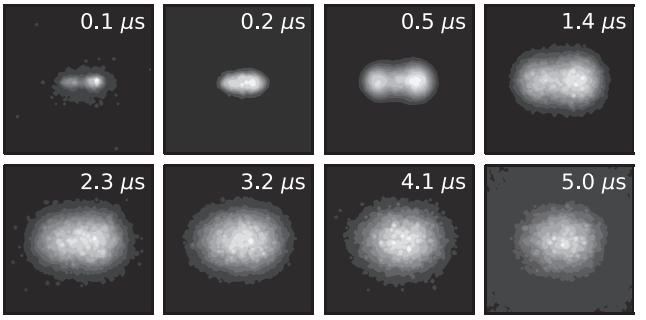

FIG. 6. Sequence of 5 mm × 5 mm images showing the time evolution of the LIP's broadband emission as captured by an intensified CCD camera.

IV. MICROWAVE SCATTERING EXPERIMENTS

Microwave scattering experiments were carried out to confirm the existence of the described resonance in the LIP at the times suggested by the optical emission measurements. A schematic of the setup for these scattering studies is shown in Fig. 7. The same experimental conditions used for the optical emission measurements were used to produce a plasma spheroid with the major axis oriented parallel to the incident electric field inside a WR62 waveguide. The incident continuous microwave signal was generated by an HP 83732A signal generator, and reflection/transmission signals were detected by Krytar 303SK crystal detectors (CDs) and recorded through an oscilloscope.

The time evolution of the reflection ($|S_{11}|^2$) and transmission ($|S_{21}|^2$) power ratios obtained from this two-port waveguide experiment is shown in Fig. 8. The data are presented as a function of Δt, which was the delay time between the laser Q-switch trigger and the time the measurement was taken. In these plots, there are two noticeable reflection peaks and corresponding transmission dips. The first appears to be due to a wave cutoff effect from a layer of weakly

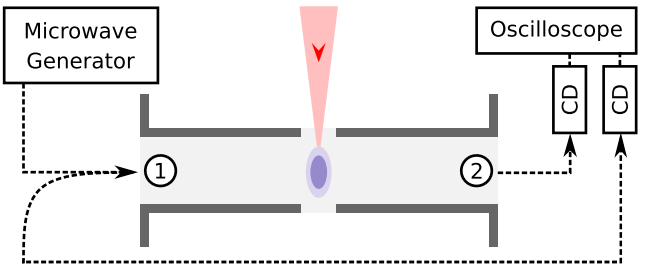

FIG. 7. Schematic of the experimental setup for Ku band microwave scattering measurements.

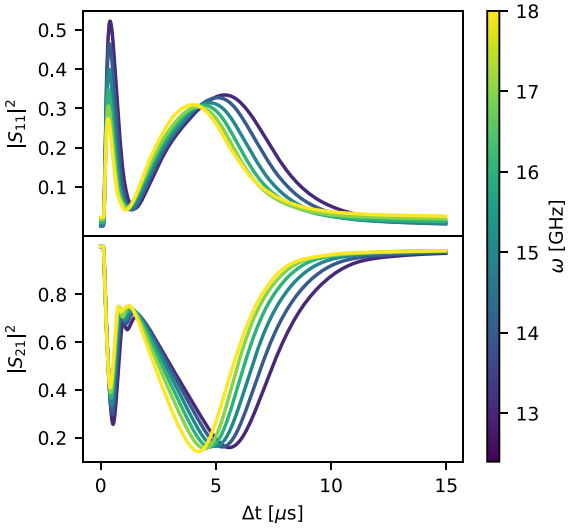

FIG. 8. Time evolution of reflection and transmission of a WR62 waveguide embedded with a single LIP element.

ionized plasma surrounding the hot plasma kernel that fills the microwave cavity at early times. This layer, referred in the literature as an ionization aureole,[19] is formed as a result of photoionization of the gas by short-wavelength radiation emitted by the central core of the LIP. The cutoff nature of this effect is further illustrated in Fig. 9, which shows plots of $|S_{11}|^2$ and $|S_{21}|^2$ vs. ω at times when the first peak is observed. The plots show a broadband increase in reflection and a corresponding decrease in transmission until $\Delta t = 0.4$ μs, when the aureole is assumed to have reached its greatest size. For $\Delta t > 0.4$ μs, reflection decreases and transmission increases at higher frequencies, leading to an apparent decrease in the cutoff frequency with time as n_e decays in the relatively short-lived aureole. It is worth noting that this n_e decay is not resolved in the Stark broadening measurements discussed above since broadening of the Hα line is dominated by the denser core plasma.

The second peak is due to a surface plasmon resonance effect, which is responsible for the Ku band scattering described in Sec. II. Plots of $|S_{11}|^2$ and $|S_{21}|^2$ vs. ω at times when the second peak is observed can be found in Fig. 10. The plots show an extinction spectrum with a minimum power ratio of ∼15% entering the Ku band at 18 GHz and moving left to lower frequencies with increasing time, i.e., decreasing n_e. A corresponding reflection spectrum precedes the extinction spectra with a peak power ratio of ∼30%, which points to an absorption value of ∼55%. The large bandwidth of the extinction and reflection spectra is expected given the relatively large size of the plasma with respect to the wavelength.[22] This trend of decreasing ω_0 (i.e., frequency of least transmission) with increasing Δt (decreasing n_e) follows the trend theorized in Eq. (5). The resonant behavior is observed at laser Q-switch delay times in the range of 4.4–5.7 μs, which is mostly within the standard error of the times predicted previously by combining the results of Figs. 3 and 5, providing further confirmation of the surface plasmon nature of this scattering effect. The small discrepancies in Δt were expected given the approximate nature of Eq. (5), the finite collisionality/size of the LIP, and the extrapolated nature of the values in Fig. 5.

The results presented provide insights into the nature of the plasmonic response of these LIP resonators. Such resonators could be used to extrapolate the functionality of solid-state Mie-based MTMs[23] to extreme conditions where energy fluxes exceed the damage threshold of solid-state materials and remote generation is advantageous. The most simple application of these resonators would be as a meta-atom in a tunable microwave or THz metasurface (MTS) mirror or absorber. Such a MTS could be generated by focusing a high-energy laser pulse through a micro-lens array and into a gas. This and other examples of all-plasma MTMs will be described in forthcoming publications.

V. SUMMARY

This paper addressed the potential use of LIPs as tunable resonators for MTM applications. A simple model was introduced to describe the scattering resonance of these near-ellipsoidal plasmas and its dependence on their eccentricity

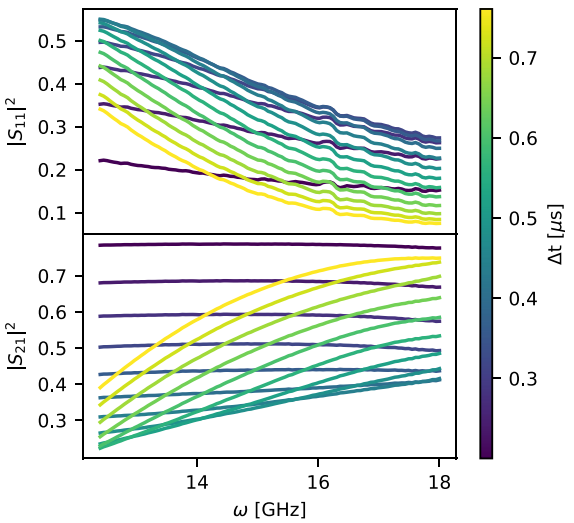

FIG. 9. Experimental reflection and transmission spectra of the ionization aureole effect.

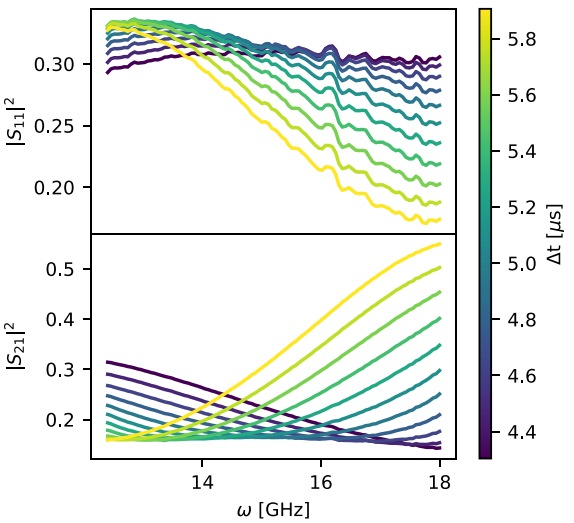

FIG. 10. Experimental reflection and transmission spectra of the surface plasmon effect.

and intrinsic plasma properties. This dependence was confirmed through Ku band transmission experiments of a waveguide with an embedded single plasma element and through detailed spectroscopic and optical diagnostics of the LIP. The described resonator has the potential to be used as the building block in a new class of MTMs with fully three-dimensional structural flexibility in the microwave and THz regime of the EM spectrum.

ACKNOWLEDGMENTS

This work was supported by the Air Force Office of Scientific Research under Award No. FA9550-14-10317. R. Colón Quiñones and T. Underwood gratefully acknowledge the financial support of the National Defense Science and Engineering Graduate Fellowship Program.

[1]D. R. Smith, J. B. Pendry, and M. C. Wiltshire, Science **305**, 788 (2004).
[2]C. Caloz and T. Itoh, *Electromagnetic Metamaterials: Transmission Line Theory and Microwave Applications* (Wiley-Interscience, 2006).
[3]H. Chen, C. T. Chan, and P. Sheng, Nat. Mater. **9**, 387 (2010).
[4]N. I. Zheludev and Y. S. Kivshar, Nat. Mater. **11**, 917 (2012).
[5]O. Sakai and K. Tachibana, Plasma Sources Sci. Technol. **21**, 013001 (2012).
[6]H. Kim, S. Parsons, and J. Hopwood, Plasma Sources Sci. Technol. **27**, 015010 (2018).
[7]K. Kourtzanidis, D. M. Pederson, and L. L. Raja, J. Appl. Phys. **119**, 204904 (2016).
[8]D.-S. Lee, O. Sakai, and K. Tachibana, Jpn. J. Appl. Phys., Part 1 **48**, 062004 (2009).
[9]R. Lee, B. Wang, and M. Cappelli, Appl. Phys. Lett. **111**, 261105 (2017).
[10]C.-H. Liu, P. Carrigan, B. J. Kupczyk, X. Xiang, N. Behdad, J. E. Scharer, and J. H. Booske, IEEE Trans. Plasma Sci. **43**, 4099 (2015).
[11]Y. Nakamura, A. Iwai, and O. Sakai, Plasma Sources Sci. Technol. **23**, 064009 (2014).
[12]C. Qu, P. Tian, A. Semnani, and M. J. Kushner, Plasma Sources Sci. Technol. **26**, 105006 (2017).
[13]O. Sakai, T. Shimomura, and K. Tachibana, Phys. Plasmas **17**, 123504 (2010).
[14]P. K. Singh, J. Hopwood, and S. Sonkusale, Sci. Rep. **4**, 5964 (2014).
[15]Z. Cohick, W. Luo, S. Perini, A. Baker, D. Wolfe, and M. Lanagan, Appl. Phys. Express **9**, 116201 (2016).
[16]S. Dennison, A. Chapman, W. Luo, M. Lanagan, and J. Hopwood, Plasma Sources Sci. Technol. **25**, 03LT02 (2016).
[17]Z. A. Kudyshev, M. C. Richardson, and N. M. Litchinitser, Nat. Commun. **4**, 2557 (2013).
[18]C. DeMichelis, IEEE J. Quantum Electron. **5**, 188 (1969).
[19]G. Ostrovskaya and A. Zaĭdel', Phys.-Usp. **16**, 834 (1974).
[20]Y.-L. Chen, J. Lewis, and C. Parigger, J. Quant. Spectrosc. Radiat. Transfer **67**, 91 (2000).
[21]H. Roskos, M. Thomson, M. Kreß, and T. Löffler, Laser Photonics Rev. **1**, 349 (2007).
[22]C. F. Bohren and D. R. Huffman, *Absorption and Scattering of Light by Small Particles* (Wiley-VCH, 1998).
[23]Q. Zhao, J. Zhou, F. Zhang, and D. Lippens, Mater. Today **12**, 60 (2009).
[24]G. Mie, Ann. Phys. **330**, 377 (1908).
[25]Y. P. Raizer, *Gas Discharge Physics* (Springer-Verlag, 1991).
[26]O. Nestor and H. Olsen, SIAM Rev. **2**, 200 (1960).
[27]K. T. Loebner, T. C. Underwood, T. Mouratidis, and M. A. Cappelli, Appl. Phys. Lett. **108**, 094104 (2016).
[28]T. C. Underwood, K. T. Loebner, and M. A. Cappelli, High Energy Density Phys. **23**, 73 (2017).
[29]H. Ehrich and D. Kelleher, Phys. Rev. A **21**, 319 (1980).